PB82-143306

# Satellite Estimation of the Surface Energy Balance, Moisture Availability and Thermal Inertia

Pennsylvania State Univ., University Park

Prepared for

Environmental Sciences Research Lab.
Research Triangle Park, NC

23 Aug 80

U.S. Department of Commerce
National Technical Information Service
NTIS.

| TECHNICAL REPORT DATA (Please read Instructions on the reverse before completi | | |
|---|---|---|
| 1. REPORT NO. EPA-600/J-81-478 | 2. Journal Article | 3. PB82-143306 |
| 4. TITLE AND SUBTITLE SATELLITE ESTIMATION OF THE SURFACE ENERGY BALANCE, MOISTURE AVAILABILITY AND THERMAL INERTIA | | 5. REPORT DATE November 1981 |
| | | 6. PERFORMING ORGANIZATION CODE 2362030 |
| 7. AUTHOR(S) T.N. Carlson, J.K. Dodd, S.G. Benjamin, and J.N. Cooper | | 8. PERFORMING ORGANIZATION REPORT NO. |
| 9. PERFORMING ORGANIZATION NAME AND ADDRESS Department of Meteorology The Pennsylvania State University University Park, Pennsylvania 16802 | | 10. PROGRAM ELEMENT NO. CDWA1A/06-0652 (FY-81) |
| | | 11. CONTRACT/GRANT NO. |
| 12. SPONSORING AGENCY NAME AND ADDRESS Environmental Sciences Research Laboratory--RTP,NC Office of Research and Development U.S. Environmental Protection Agency Research Triangle Park, North Carolina 27711 | | 13. TYPE OF REPORT AND PERIOD COVERED |
| | | 14. SPONSORING AGENCY CODE EPA/600/09 |
| 15. SUPPLEMENTARY NOTES REFERENCE: Journal of Applied Meteorology, 20(1):67-87, January 1981. | | |

16. ABSTRACT

A method for inferring the distribution of surface heat and evaporative fluxes and the ground moisture availability and thermal inertial (ground conductive capacity) is used to analyze two urbanized areas, Los Angeles and St. Louis. The technique employs infrared satellite temperature measurements in conjunction with a one-dimensional boundary-layer model. Results show that there is a marked reduction of evaporation and moisture availability and a corresponding elevation of sensible heat flux over urbanized areas and over cropped areas with low vegetative cover. Conversely, low heat flux and high evaporation characterize vegetated and, especially forested areas. Warm urban centers appear directly related to a reduction in vegetation, which normally allows for a greater fraction of available radiant energy to be converted into latent heat flux. The distribution of thermal inertia was surprisingly ill-defined and its variation between urban and rural areas was quite small. Thus, the increased heat storage within the urban fabric, which has been proposed as the underlying cause of the nocturnal heat island, may be caused mainly by enhanced daytime surface heating which occurs because of surface dryness, rather than by large spatial variations in the conductivity of the surface.

| 17. KEY WORDS AND DOCUMENT ANALYSIS | | |
|---|---|---|
| a. DESCRIPTORS | b. IDENTIFIERS/OPEN ENDED TERMS | c. COSATI Field/Group |
| | | |
| 18. DISTRIBUTION STATEMENT RELEASE TO PUBLIC | 19. SECURITY CLASS (This Report) UNCLASSIFIED | 21. NO. OF PAGES |
| | 20. SECURITY CLASS (This page) UNCLASSIFIED | 22. PRICE |

EPA Form 2220-1 (Rev. 4-77) PREVIOUS EDITION IS OBSOLETE

REPRODUCED BY
NATIONAL TECHNICAL
INFORMATION SERVICE
U.S. DEPARTMENT OF COMMERCE
SPRINGFIELD, VA 22161

EPA-600/J-81-478
Journal Article

Reprinted from JOURNAL OF APPLIED METEOROLOGY, Vol. 20, No. 1, January 1981
American Meteorological Society
Printed in U. S. A.

# Satellite Estimation of the Surface Energy Balance, Moisture Availability and Thermal Inertia

TOBY N. CARLSON, JOSEPH K. DODD,[1] STANLEY G. BENJAMIN AND JAMES N. COOPER

*Department of Meteorology, The Pennsylvania State University, University Park 16802*

(Manuscript received 17 March 1980, in final form 23 August 1980)

ABSTRACT

A method for inferring the distribution of surface heat and evaporative fluxes and the ground moisture availability and thermal inertia (ground conductive capacity) is used to analyze two urbanized areas, Los Angeles and St. Louis. The technique employs infrared satellite temperature measurements in conjunction with a one-dimensional boundary-layer model. Results show that there is a marked reduction of evaporation and moisture availability and a corresponding elevation of sensible heat flux over urbanized areas and over cropped areas with low vegetative cover. Conversely, low heat flux and high evaporation characterize vegetated and, especially, forested areas. Warm urban centers appear directly related to a reduction in vegetation, which normally allows for a greater fraction of available radiant energy to be converted into latent heat flux. The distribution of thermal inertia was surprisingly ill-defined and its variation between urban and rural areas was quite small. Thus, the increased heat storage within the urban fabric, which has been proposed as the underlying cause of the nocturnal heat island, may be caused mainly by enhanced daytime surface heating which occurs because of surface dryness, rather than by large spatial variations in the conductivity of the surface.

## 1. Introduction

One of the most notable meteorological anomalies produced by human activity is the urban heat island. Many studies (e.g., Duckworth and Sandberg, 1954; Landsberg, 1956; Oke, 1968; Chandler, 1976) show urban-rural temperature differences of several degrees Celsius with the greatest elevations in ground and air temperatures occurring during the evening hours. Recent investigations into the phenomenon have begun to focus attention on the significance of differential heating patterns in altering the amount and type of precipitation surrounding urban areas. Earlier studies of urban precipitation anomalies led to various hypotheses concerning the possible anthropogenic effects on the weather (Changnon, 1969). The results of METROMEX (Braham and Dungey, 1978; Braham and Wilson, 1978; Huff and Vogel, 1978; Changnon, 1969, 1978) indicate that there are significant precipitation anomalies in the vicinity of St. Louis, which are connected with convective situations during the summer months. Moreover, these studies show clearly that strong convergence of the low-level wind occurs over the hottest portions of the city (Kropfli and Kohn, 1978; Wong and Dirks, 1978; Shreffler, 1979). Both observational and theoretical investigations indicate that surface heat flux must be considered in modeling small-scale circulation patterns in regions of differential surface heating.

Models capable of predicting the surface temperature response and the amount of surface heating are in wide use, both as components within larger hydrodynamic models or as separate one-dimensional entities whose purpose is to study the nature of surface heating by itself. Various types of one-dimensional surface temperature models have been developed [see, e.g., Myrup (1969), Outcalt (1972), Rosema (1979), Carlson and Boland (1978, hereafter referred to as CB), Deardorff (1978), Blackadar (1979) and Soer (1977; 1980)].

In applying any model, however, it is possible to simulate any desired surface temperature response by appropriately setting the model parameters. Over heterogeneous terrain such as an urban-rural complex, the concepts of conductivity or moisture availability are difficult to measure directly. Yet, it is certainly evident that the ability of a particular surface to transpire or to conduct heat internally must be represented in a physically realistic manner in order to predict the surface temperature. Certainly, radiometric surface temperature observations over urban and rural areas indicate that the surface heating is strongly influenced by the composition of the surface.

In many numerical models of the surface, an important constraint imposed on the solution of the

[1] Present affiliation: Aerospace Corporation, Los Angeles, CA 90009.

0021-8952/81/010067-21$09.25
© 1981 American Meteorological Society

thin transition layer between the air and the surface interface, across which diffusive fluxes at the interface are passed to the turbulent layer, and a 1 m ground layer (Fig. 1). The transition layer is viewed as a layer that contains many surface obstacles. Across the layer there is a variation between purely turbulent and purely molecular flow where radiation, conduction and turbulent heat transfer coexist in some fashion.

The underlying constant in the model is the energy balance at the surface air interface

$$R_n = G_0 + H_0 + E_0 = (1 - A_0)S - \epsilon_g\sigma T_0^4 + \epsilon_a\sigma T_a^4, \quad (1)$$

where $G_0$, $H_0$ and $E_0$ represent, respectively, the sensible heat flux into the ground, the sensible heat flux into the atmosphere; and the latent heat flux into the atmosphere. Net radiation $R_n$ is calculated from a radiation balance at the surface [the right side of (1)], where $A_0$ is the surface albedo, $T_0$ the temperature at the ground air interface, $\sigma$ the Stephan-Boltzmann constant, and $T_a$ the temperature at the top of the surface layer ($z$ = 50 m). Net solar flux (direct plus diffuse) $S$ is calculated from a one-layer solar-radiation model (Carlson and Boland, 1978). Emissivity at the ground is set equal to 1.0, but that for the atmosphere $\epsilon_a$ is calculated from a formula suggested by Monteith (1961) in which thermal back radiation is represented as a function of the total precipitable water $\omega$ in the atmospheric column, $\epsilon_a = 0.725 + 0.17 \log_{10} \omega$, where $\omega$ is in centimeters. Surface flux of sensible heat is parameterized in the surface layer, over which $H_0$ is presumed to be constant, as

$$H_0 = -(C_h + \rho c_p K_h)\frac{\partial\theta}{\partial z}, \quad (2)$$

where $K_h$ is the eddy diffusivity, $C_h$ a heat transfer coefficient for nonturbulent heat flux in the surface transition layer, $c_p$ the specific heat at constant pressure for dry air, and $\rho$ the air density. The potential temperature $\theta$ is normalized to surface pressure at the ground-air interface; thus $\theta_0 = T_0$. Integrating (2) with respect to $z$ from the ground to the top of the surface layer at $z_a$, where $\theta = \theta_a$ yields

$$\theta_0 \equiv T_0 = \theta_a + H_0 I_h/\rho c_p, \quad (3)$$

where $I_h$ is essentially a resistance coefficient determined from an integration of the generalized height-dependent diffusivity $K(z) = K_h + C_h/\rho c_p$.

A similar equation to (3) for water vapor flux is

$$E_0 = \frac{\rho L_e}{I_q} M[q_{0s}(T_0) - q_a], \quad (4)$$

where $I_q$ for water vapor is identical to that for heat except that the diffusivities refer to those of water vapor, $K_q$ and $C_q$. In all calculations $K_q$ was assumed

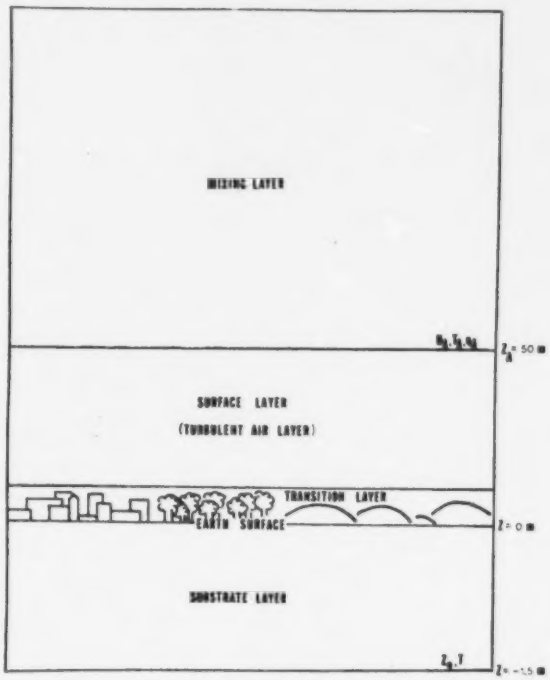


FIG. 1. Basic structure of model.

to be equal to $K_h$, but $C_h$ and $C_q$ were assigned, for lack of a better choice, values for the molecular diffusivities of heat and water vapor. Justification for use of molecular diffusivity in the context is discussed by Garratt (1978). Here, $q_{0s}(T_0)$ and $q_a$ are, respectively, the saturation specific humidity at the surface and the specific humidity at $z_a$, the top of the surface layer; $L_e$ is the latent heat of vaporization, and $M$ is called the *moisture availability*. The concept of moisture availability was suggested by Tanner and Pelton (1960) and later elaborated on by Nappo (1975). This parameter basically expresses the efficiency of surface evaporation and is the fraction of maximum possible evaporation for a saturated surface at temperature $T_0$. The moisture availability can be conceived as a measure of water saturation at ground surface. For vegetation, $M$ is related to the internal resistance (bulk stomatal diffusion resistance) discussed by Monteith (1975).

The ground surface flux $G_0$ is given by the standard conduction equation

$$G_0 = \lambda(T_0 - T_{-1})/\Delta Z, \quad (5)$$

where $\lambda$ is the thermal conductivity of the substrate and $T_{-1}$ the temperature of the first substrate level, a distance $\Delta Z$ below the ground surface. The transfer of heat through the soil is governed by the diffusion equation. Assuming a homogeneous substrate layer,

and $l$ was arbitrarily chosen as 28 m in the surface layer. In the layers above the surface, the local Richardson number is calculated as

$$\mathrm{Ri} = \frac{g}{\bar{\theta}\Delta z}\frac{(\theta_i - \theta_{i-1})}{S_i^2}, \quad (14)$$

while the critical Richardson number ($\mathrm{Ri}_c$) is calculated as a function of the geostrophic wind speed using an empirical result suggested by Blackadar[2]

$$\mathrm{Ri}_c = 0.5542 \exp\{-[0.2129(u_{gi}^2 + v_{gi}^2)^{1/2}] + 0.2\}, \quad (15)$$

where $u_{gi}$ and $v_{gi}$ are the geostrophic wind speed components in meters per second. When the local Richardson number exceeds the critical value, turbulent exchange will cease at that height and $K_i$ is arbitrarily set equal to zero.

The lowest 50 m layer must be treated differently as there will be no turbulent exchange through the underlying surface. Accordingly, the last term in each equations (10) and (11) must be replaced by $-u_*^2 u_1/W_A\Delta z$ and $H_0/c_p\rho\Delta z$, respectively, which are the surface boundary flux conditions.

### c. *Initial conditions*

The temperature at the bottom of the 1 m ground slab was set equal to constant, which was a representative climatological value. Above the surface layer, the mixing layer of depth $h$, potential temperature $\theta_n$ and mixing ratio $q_n$ were allowed to vary during the daytime according to a model of Tennekes (1973) in which the mixing-layer parameters responded to an addition of sensible heat flux from the ground and an entrainment of higher potential temperature from above the mixing layer. Thus, the temperature and moisture at the top of the surface layer were determined by the amount of surface heating and the stability and moisture distribution above the surface layer. The wind speed $u_n$, however, was not calculated from Eq. (10). Instead, a 500 m layer above the surface layer was presumed to be well mixed with $u_n$ constant up until the time of late afternoon stability reversal, a reasonable assumption for a clear sunny day. The nighttime model became effective when $H_0$ became zero in the late afternoon; subsequently, the wind and temperature profiles were calculated from (10) and (11) over the 500 m deep layer at equal intervals of 50 m from $i = 1$ at $z_n$ to $i = 10$ at $z = 500$ m (Fig. 2). Although the model was usually started near dawn, the initial wind profile was determined from a late afternoon or early evening wind sounding when the stability would have been close to neutral. The procedure for initializing the wind profile and for obtaining $u_n$ was as follows: The vertical shear of the geostrophic wind was determined from an analysis of local surface fields of temperature and pressure; usually only one or two additional wind observations above the surface layer were available in the lowest 500 m. In order to fit a wind profile to the observations, free convection scaling was assumed to govern the wind profile prior to the vanishing of the upward heat flux. The assumption of free convection scaling assumes that turbulence in the lower part of the mixed layer is buoyantly driven (Tennekes, 1970), and provides a relationship for the wind shear

$$\frac{\partial V}{\partial z} = b' z^{-4/3}. \quad (16)$$

This leads to a velocity defect expression

$$V - V_{\mathrm{obs}} = b'(z^{-1/3} - z_{\mathrm{obs}}^{-1/3}), \quad (17)$$

where $b'$ is determined empirically and $z$ is measured downward from $z_{\mathrm{obs}}$, the level where the wind speed $V$ is equal to $V_{\mathrm{obs}}$. Eq. (17) is applied to 0000 GMT wind data for the layer between the top of the surface layer at 50 m and $z_{\mathrm{obs}}$ which was taken at 200 m. The wind at 200 m was either a measured wind close to that level or was assumed to be equal to the surface geostrophic wind. Above 200 m the wind was assumed to be initially constant with height to 500 m. The specified initial wind profile may possess a significant ageostrophic component, but the model has been found to adjust smoothly to the transition during the first hour or two of integration beyond the time of reversal in the sign of the heat flux, ultimately achieving a quasi-equilibrium with small accelerations.

### d. *Solution of the model*

During the daytime the surface heat flux is obtained by a solution to the surface energy budget (1). The temperature at the surface is determined from the heat flux in accordance with the stability prescribed by (3). Given prescribed values for all of the terrain parameters and an initial temperature and wind profile within the atmosphere above the surface and within the ground, the essential unknowns $H_0$, $T_0$, $T_{-1}$, $E_0$ and $G_0$ can be found using Eqs. (1), (3), (4), (5) and (6). Because many of the terms are interdependent, it was necessary to cycle through the system of equations until convergence was achieved. Values of the eddy diffusivities were cal-

[2] Private communication. This relationship is based on a comparison of field measurements of wind made at O'Neill, Nebraska, and Wangara with those obtained from the Blackadar (1979) slab model. Under light wind conditions there is a greater likelihood of finding thin layers where wind shear and temperature vary rapidly with height. If $\Delta z$ is too large to resolve this, the calculated Ri may be far larger than the smallest value in the layer and thus turbulence can still occur even though the calculated $\mathrm{Ri} > 0.2$. The equation systematically accounted for the bias found when the measurements were compared with the model results.

$$\lambda[\text{cal cm}^{-1}\ \text{K}^{-1}\ \text{s}^{-1}] = -0.00013 + 0.0502P + 1.21P^2[\text{cal cm}^{-2}\ \text{K}^{-1}\ \text{s}^{-1/2}] \quad (20)$$

was used as a constraint on the value of $\lambda$ in the model.[3] Eq. (20) was determined by fitting a second-order regression equation through 20 pairs of $\lambda$ and $P$ values listed in Sellers (1965) and in the *Manual of Remote Sensing, II* (1975). The regression was found to explain 91% of the variance of $\lambda$ about $P$ in the dependent data sample, providing an empirical result which corresponds to a wide variety of surface materials. In fact, the actual surface canopy may consist of materials which may not represent a truly diffusing or conducting medium, such as a mixture of structures and vegetation—trees, roads, houses, crops, etc.

It is customary in surface layer modeling to specify the terrain parameters in order to calculate the surface temperature and the surface energy fluxes. Although we have shown that this can be done, it is the purpose of this paper to demonstrate how the model can be used to infer values for $M$ and $P$ and the surface fluxes, given measurements of the surface temperature. CB show that by supplying two surface temperatures in the same temperature cycle, two terrain parameters could be treated as unknowns whose values could be inferred with some uniqueness from iterative solutions of the mode. The method for inverting the model to obtain the terrain parameters given the surface temperatures is described in Section 4.

## 3. Reduction and analysis of satellite temperature measurements

During the past decade, several meteorological satellites with the capacity to provide high-resolution thermal mapping of the earth's surface have been placed in orbit. Polar orbiting vehicles, however, are incapable of scanning more than twice in a diurnal temperature cycle, and, until recently, the passes were made at hours shortly after sunrise and sunset. On 26 April 1978, the Heat Capacity and Mapping Mission (HCMM) polar-orbiting satellite was launched by NASA to provide high-resolution (~600 m) measurements of the radiometric ground temperature for application to ground-sensing problems. The noise equivalent temperature error (NE$\Delta T$) for this satellite is considered to be 0.3 K.[4] This satellite was able to scan a given location twice a day (at intervals of 16 days) at times very close to those of local maximum and local minimum temperature, approximately 1330 and 0230 LST, respectively. [More recently, the polar orbiting TIROS-N was launched into an orbit which allows for data acquisiton at about 1500 and 0300 LST and has a resolution of ~1100 m at zero scan angle (satellite directly overhead) and a NE$\Delta T$ of 0.1 K.]

Satellite detection of heat islands has become possible only since the recent advent of high-resolution infrared window measurements. Although techniques for performing densitometric or radiometric analyses of small-scale temperature variations from aircraft date have been applied widely to the study of urban and other types of terrain (*Manual of Remote Sensing, II*; 1975); Rao (1972) was the first person to publish an account of the heat island using satellite data. Recently, it has been shown (Carlson *et al.*, 1977; Matson *et al.*, 1978) that the heat island is a relatively widespread phenomena.

The procedure which we followed for taking the raw HCMM satellite radiance data and coverting the information to temperature maps on a fixed geographical grid was as follows:

1) Digital count information for an area covered by a 512 × 512 matrix of data points (pixels) was extracted from raw data tape.

2) A 130 × 130 working area (~80 km on a side) was selected from within the larger matrix. A histogram of the count value was made and the data field printed out as an alphanumeric character map; an example of the type of output is shown by Chen *et al.* (1979).

3) Inspection of the character map compared with a topographic map enabled us to identify specific geographic features within the working area. These features were assigned values of $x$, $y$ coordinates within an arbitrary geographically fixed reference frame which we call the "topo" grid.

4) The digital count (DN) values were converted to temperature using the appropriate calibrations. A spatially constant water vapor correction (Cogan and Willand, 1976) was applied. Moisture data was obtained from radiosonde information taken within or near the city.

5) Temperature analyses for both the daytime and night time orbits were rectified to the topo coordinates. A pair of temperatures, one day and one night value, were located at each $x$, $y$ coordinate of a subset area.[5] All analyses were subjected to a simple one-pass smoothing.

## 4. Combining of model output with satellite data

As mentioned in Section 1, satellite temperature measurements were used in conjunction with

[3] In some papers thermal inertia is presented in thermal inertia units (TIU), which are W m$^{-2}$ K$^{-1}$ s$^{1/2}$. Approximately 400 TIU are equivalent to 0.01 cal cm$^{-2}$ K$^{-1}$ s$^{-1/2}$, the units presented in this paper.

[4] The authors recently became aware of a temperature offset error of ~5°C which must be added to all the HCMM temperature measurements to make them correct. Further analyses with the corrected temperatures indicate that the values of $M$ and $E_0$ should be somewhat smaller and the value of $P$ and $H_0$ somewhat larger than reported in this paper, although because of the energy balance constraint, the patterns appear little affected by making this correction.

[5] The location error of the data within the "topo" grid is about ±1 pixel (~600 m for HCMM).

tions was always close to 1.0. In instances of bivalued solutions, there was very little variation of $X$ with temperature. Thus, except for isolated occasions with extreme values of $M$ of $P$, the solutions were single valued.

Accordingly, the last step in the analysis procedure, as illustrated by the flow chart in Fig. 3, was to transform the rectified temperature images contained in the subset grid to maps of $M$, $P$, $H_0$ and $E_0$ ($G_0$ is henceforth not discussed). The transformation was done by substituting the measured temperatures into the regression equations for all grid points in the topo array. Because the day and night orbits were not exactly coincident, the topo subset area common to both working areas was necessarily smaller than either 130 × 130 working area, as illustrated in Fig. 4.

In initializing the model, the choice of surface parameters, other than $M$ and $P$, and of the meteorological data was not critically important in determining $T_0$, although reasonable values of the wind speed, surface roughness, surface albedo, temperature, etc., were chosen to assure that the inferred values of $M$ and $P$ lay within reasonable limits for the observed ranges of daytime and nighttime temperatures.[7]

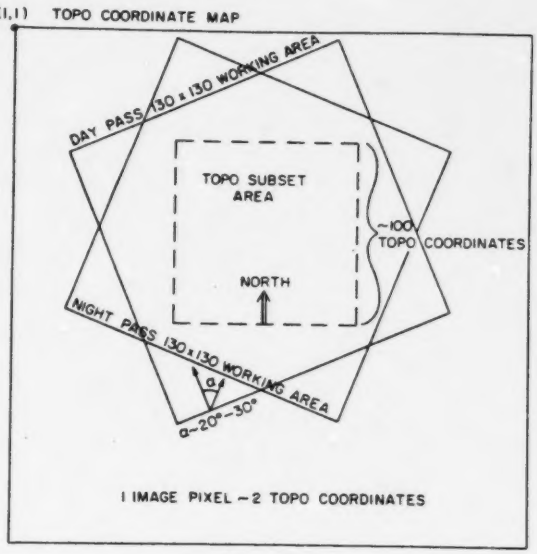


FIG. 4. Schematic representation of subset area.

## 5. Case studies

Satellite measurements for the two cases presented in this paper were obtained from two night/day pairs, 36 h apart over Los Angeles (30–31 May 1978) and St. Louis (9–10 June 1978). Nighttime orbits were made at about 0230 LST on the first day and daytime orbits at about 1330 LST on the following afternoon. Since the daytime temperature wave produces an effect on the nighttime temperature, simulations were always initiated at about 0600 LST model time. However, in order to minimize computer time, and because it is unrealistic to expect a one-dimensional model to give satisfactory results for periods much in excess of one day, we made the assumption that the surface temperature wave was stationary over a period of 36 h. We assumed stationarity in the temperature response between 30 and 31 May as a basis for reversing the ordering of day/night sequence in the model and for assuming a 12 h interval between orbits. In the Los Angeles case, the model was initialized at dawn on the 30th and allowed to proceed until nearly dawn on the 31st. However, the satellite passes were made at approximately 0230 LST 30 May and 1330 LST 31 May. In the St. Louis case the model was run for 36 h starting at dawn on 9 June, with daytime output during the afternoon of the 10th. The satellite passes were made at approximately 0230 LST 9 June and 1330 LST 10 June.

Justification for the artificial arrangement of orbits is based not simply on necessity but on the grounds that surface temperature under uniform weather conditions responds most sensitively to the nature of the terrain. Meteorological conditions were typical in both cases of a dry, mild, fair weather pattern with clear skies and weak advection; no rain had occurred for several days prior to the period. In looking at a number of other urban cases at different times of the year, we are struck by the overall similarity in surface-temperature patterns that characterize a particular urban area. The recurrence of these patterns suggests that surface effects more than the large-scale weather conditions govern the small-scale patterns of temperature under normal circumstances. Thus, we conclude that no serious complications arose from the reverse ordering of orbits.

### *a. Los Angeles 30 and 31 May 1978*

The daytime (1330 LST 31 May) surface temperature map in Fig. 5 displays a large area centered on the cities of Maywood and Commerce where the ground temperatures were in excess of 32°C, warmer than at any other location within the Los Angeles Basin. Highest values, in excess of

[7] The value of the surface roughness $z_0$ used in these urban cases was 30 cm. Jason Ching of the Environmental Protection Agency has calculated from tower wind data from St. Louis a roughness length of between 60 and 120 cm. Our choice of 30 cm is likely to be close to an area average and well within an order of magnitude of the extreme values for the St. Louis area. We also chose a surface albedo of 18% which, according to our visible radiance measurements from the satellite, was within ±5% of the extreme values over most of the region.

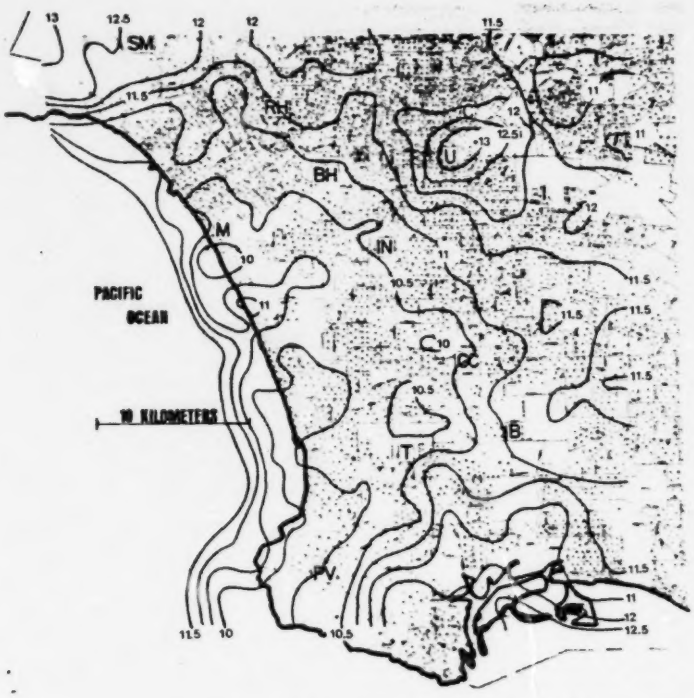


FIG. 6. Los Angeles, 30 May 1978 nighttime (~0230 LST) surface temperature analysis. Units in °C.

FIG. 7. Los Angeles moisture availability analysis for 30–31 May 1978.

FIG. 9. Los Angeles surface sensible heat flux (W m$^{-2}$ × 0.1) at approximately 1330 LST 31 May 1978 ($R_n \approx 630$ W m$^{-2}$).

FIG. 10. Los Angeles surface moisture flux (W m$^{-2}$ × 0.1) at approximately 1330 LST 30–31 May 1978 ($R_n \approx 630$ W m$^{-2}$).

FIG. 12. St. Louis, 9 June 1978 nighttime (~0230 CST) surface temperature analysis. Units in °C.

was relatively small, yet $E_0$ still exhibits values there which are as large as $H_0$ in regions where the latter is a maximum.

*b. St. Louis, 9 and 10 June 1978*

The map of daytime temperature (Fig. 11) displays a wide variation, with values ranging from 23°C to above 32°C. The three urban sites which show the highest temperatures include downtown St. Louis (D), East St. Louis across the river (E), and the industrial center of Granite City (G). Over these areas the ground temperatures varied from 30 to 34°C. Maximum temperatures were located near the City Hall and Memorial Plaza district where high-rise office buildings, parking lots, and a dense network of roads and highways comprise an urban ground fabric with little vegetation. Both East St. Louis and Granite City are also completely developed, with significant areas of heavy industry. Several other non-urban sites (identified by the letter C) exhibit daytime temperatures approaching or exceeding 30°C. All of these sites are separated from the urban centers by several kilometers and are located to the northwest, northeast and southeast of the city. Examination of U.S. Geological Survey land-use maps indicates that these areas consist of cropland (probably in an early stage of maturity) and pasture characterized by extensive areas of open field and low vegetation.

The water bodies [e.g., Horseshoe Lake (H)] are well defined by isopleths of lower temperature with the lowest isotherm being 23°C. Although actual river and lake temperatures varied from 15 to 19°C in the raw measurements, the smoothing of the data combined with the elimination of isotherms below a certain value tended to remove detail from the analysis around bodies of water such as the Mississippi River. The most evident ground temperature minima were centered in the southwest corner of the map (F) where a large expanse of deciduous trees remains despite the proximity of urbanization.

The nighttime range of temperature (3.5–6.5°C) presented in Fig. 12 indicates much smaller urban-versus-rural differences that those observed during the day. The St. Louis urban center possessed the highest temperatures. Values were above 6°C over the downtown area near the river, while in a significant region surrounding this area they exceeded 5.5°C. In comparison, typical rural temperatures varied from 4 to 5°C. The urban sites of East St. Louis (E) and Granite City (G), which correspond to

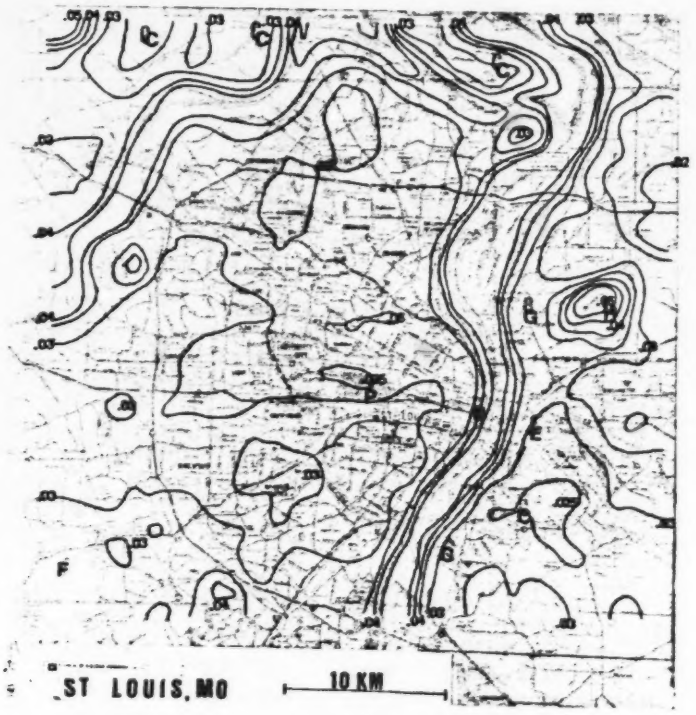


FIG. 14. St. Louis thermal inertia analysis for 9–10 June 1978 (units in cal $cm^{-2}$ $K^{-1}$ $s^{-1/2}$).

substrates impose on the energy balance compared with suburban or densely vegetated areas. The other maxima appear at the cropland sites (C) that surround the suburbs of the city. The magnitude of $H_0$ appears as large at these locations as in the most built-up areas, where values also exceeded 250 W $m^{-2}$. For most of the area outside the heavily urbanized areas $H_0$, varied from 150 to 200 W $m^{-2}$, with the smallest heat flux located over vegetated areas such as the forested region (F) southwest of the city.

The map of surface moisture flux $E_0$ (Fig. 16) displays a distribution that closely corresponds to the fields of moisture availability and sensible heat flux shown in Figs. 13 and 15. The downtown area (D) exhibits a strong minimum where an isopleth encloses a region over which $E_0$ is <260 W $m^{-2}$. This is the same area where $M$ was smallest and $H_0$ largest. The two other large urban sites (E, G) and the cropland-pasture areas (C) also appear as relative minima of $E_0$, reflecting the strong influence which vegetation exercises on the surface energy balance. The moisture flux was largest over vegetation such as the forested area southwest of the city where $E_0$ exceeded 500 W $m^{-2}$. Interestingly, as was the case with Los Angeles, the smallest values of $E_0$ were larger than the maximum sensible heat flux, suggesting that the vegetation cover over urban areas is still sufficient to provide ample moisture flux.

## 6. Discussion

The maps of temperature, moisture availability, thermal inertia, and daytime heat and moisture flux across the areas centered on the cities of Los Angeles and St. Louis should aid in understanding the mechanisms responsible for the creation and maintenance of the urban heat island. The daytime spatial variation of temperature is especially impressive with the city centers as much as 10°C warmer than nearby rural areas. Both St. Louis and Los Angeles exhibit well-defined maxima centered on the commercial and industrial districts near the downtown areas, a pattern which reflects the strong influence that land use plays in influencing the surface response to the solar forcing. Temperature minima consistently appear in locations with significant vegetation. Various grasscovered hilly areas scattered across the Los Angeles Basin and the forested region southwest of St. Louis all appear as sites where the surface temperature was distinctly lower than over urban areas just a few kilometers away.

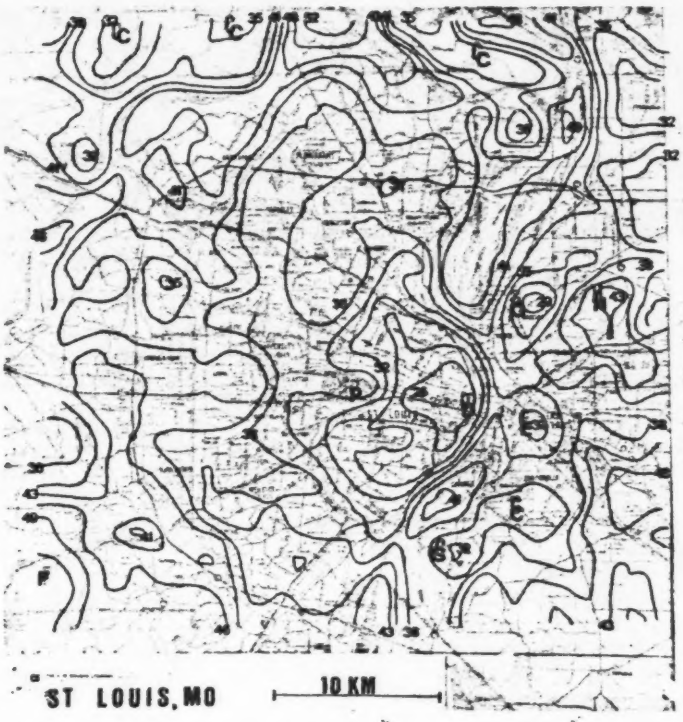


FIG. 16. St. Louis surface moisture flux (W $m^{-2}$ × 0.1) at approximately 1330 CST 10 June 1978 ($R_n \approx 640$ W $m^{-2}$).

of $H_0$ in excess of 250 W $m^{-2}$ and Bowen ratios of about 1.0, while over densely vegetated areas $H_0$ was below 100 W $m^{-2}$ and the Bowen ratio ~ 0.2. The complexity of the heat flux pattern is evident in the unsmoothed enlargement of the St. Louis downtown district (Fig. 17) where Forest Park (FP) is seen to have a heat flux roughly half that of the city center just a few kilometers away.

Over St. Louis, analyses show that the largest daytime heat flux values occurred over a corridor lying between the southern business district of St. Louis and Granite City to the northeast, the same area where METROMEX investigators found the strongest boundary-layer convergence (Kropfli and Kohn, 1978; Wong and Dirks, 1978) and the location of the earliest radar echoes and most disturbed convective situations during conditions of air mass thunderstorms (Braham and Dungey, 1978, Braham and Wilson, 1978). Thus, seems quite likely that urban precipitation anomalies are closely linked to the pattern of surface heating.

## 7. Conclusions

A procedure has been developed which uses satellite-derived surface temperature fields in combination with output from a numerical model of the boundary layer to infer the spatial distribution of the effective surface parameters, $M$ (moisture availability) and $P$ (thermal inertia), and the sensible and evaporative heat fluxes at the surface. The approach is general and may be applied to any surface for which ground temperature data is available and over which horizontal homogeneity of large-scale meteorological features may be assumed. Maps of $M$, $P$, and the sensible and latent heat fluxes at the surface are presented for two urban cases, Los Angeles and St. Louis.

$P$ and $M$ have been proposed as the two parameters that are most responsible for the temperature variations over a rural-urban complex (Carlson and Boland, 1978). The present research suggests that $M$ is the governing parameter during the day, when urban centers coincide with distinct minima and suburban and rural areas possess values in excess of 0.5. The areas of daytime temperature maxima all correspond quite closely to minima in moisture availability. However, thermal inertia patterns were surprisingly ill-defined. We had anticipated that both Los Angeles and St. Louis would exhibit maxima in $P$, reflecting the enhanced ability of the urban substrate to store and conduct heat. Although both cities were relatively warm at night, $P$ did not exhibit significant elevations in either location. Thus, the ele-

for geologic mapping by remote sensing. *J. Geophys. Res.*, **82**, 1673–1680.

Kropfli, R. A. and N. M. Kohn, 1978: Persistant horizontal rolls in the urban mixed layer as revealed by dual-Doppler radar. *J. Appl. Meteor.*, **17**, 669–676.

Landsberg, H. E., 1956: *The Climate of Towns in Man's Role in Changing the Face of the Earth*. The University of Chicago Press, 584–606.

*Manual of Remote Sensing II*, 1975: American Society of Photogrammetry, Falls Church, VA, 867 pp.

Matson, M., E. P. McClain, D. McGinnis, Jr., and J. Pritchard, 1978: Satellite detection of urban heat islands. *Mon. Wea. Rev.*, **106**, 1725–1734.

Mellor, G. L. and T. Yamada, 1974: A hierarchy of turbulence closure models for planetary boundary layers. *J. Atmos. Sci.*, **131**, 1791–1806.

Monteith, J. L., 1961: An empirical method for estimating long-wave radiation exchanges in the British Isles. *Quart. J. Roy. Meteor. Soc.*, **87**, 171–179.

Monteith, J. L., 1975: *Vegetation and the Atmosphere*, Vol. I, *Principles*. Academic Press, 278 pp.

Myrup, L. O., 1969: A numerical model of the urban heat island. *J. Appl. Meteor.*, **8**, 908–918.

Nappo, C. J., 1975: Parameterization of surface moisture and evaporation rate in a planetary boundary layer model. *J. Appl. Meteor.*, **14**, 289–296.

Oke, T. R., 1974: Review of urban climatology, 1968–1973. WMO Tech. Note, No. 134, 61 pp.

Outcalt, S. I., 1972: The development and application of a simple digital surface-climate simulator. *J. Appl. Meteor.*, **11**, 629–636.

Rao, P. K., 1972: Remote sensing of urban heat islands from an environmental satellite. *Bull. Amer. Meteor. Soc.*, **53**, 647–648.

Rosema, A., 1979: A mathematical model for simulation of the thermal behavior of bare soils, based on heat and moisture transfer. Netherlands Tech. Memo. Series, Publ. No. 11, Delft, The Netherlands.

Sellers, W. D., 1965: *Physical Climatology*. The University of Chicago Press, 272 pp.

Soer, G. J. R., 1977: The Tergra model, a mathematical model for the simulation of the daily behavior of crop surface temperature and actual evapotranspiration. Netherlands Tech. Memo. Series, Publ. No. 46, Delft, The Netherlands.

——, 1980: Estimation of regional evapotranspiration and soil moisture conditions using remotely sensed crop surface temperatures. *Remote Sensing Environ.*, **9**, 27–45.

Shreffler, J., 1979: Urban-rural differences in tower-measured winds, St. Louis. *J. Appl. Meteor.*, **18**, 829–835.

Tanner, C. B., and W. G. Pelton, 1960: Potential evapotranspiration estimates by the approximate energy balance method of Penman. *J. Geophys. Res.*, **65**, 3391–3412.

Tennekes, H., 1970: Free convection in the turbulent Ekman layer of the atmosphere. *J. Atmos. Sci.*, **27**, 1027–1034.

——, 1973: A model for the dynamics of the inversion above a convective boundary layer. *J. Atmos. Sci.*, **30**, 558–567.

Wong, K. K. and R. A. Dirks, 1978: Mesoscale perturbations on airflow in the urban mixing layer. *J. Appl. Meteor.*, **17**, 677–688.